Diffractive Pupil Telescope for high precision Space Astrometry

Olivier Guyon[a,b], Eduardo Bendek[a], Mark Ammons[a], Michael Shao [c], Stuart Shaklan [c], Robert A. Woodruff and Ruslan Belikov [d]

[a] Steward Observatory, University of Arizona, 933 N. Cherry Ave, Tucson, AZ 85721, USA;
[b] Subaru Telescope, National Astronomical Observatory of Japan, 650 N. A'ohoku Plane, Hilo, HI 96720, USA;
[c] Jet Propulsion Laboratory, 4800 Oak Grove Drive, Pasadena, CA 91109, USA;
[d] NASA Ames Research Center, Moffett Field, CA 94035, USA

ABSTRACT

A concept for high precision astrometry with a conventional wide field telescope is presented, enabling a space telescope to perform simultaneously coronagraphic imaging of exoplanets, astrometric measurement of their orbits and masses, and deep wide field imaging for a wide range of astrophysical investigations. Our concept uses a diffractive telescope pupil (primary mirror), obtained by placing a regular grid of small sub millimeter spots on the primary mirror coating. When the telescope is pointed at a bright star, the wide field image contains both a large number of background stars used for astrometric referencing, and faint diffraction spikes created by the grid of dots on the primary mirror. The diffraction spikes encode instrumental astrometric distortions due to optics or the detector, allowing precise measurement of the central star against a large number of faint background stars. With up to a few percent of the primary mirror area covered by the dots, the fraction of the central starlight located in the diffraction spikes is kept sufficiently small to allow full sensitivity deep imaging over the telescope's field of view. Since the dots are regularly spaced, they do not diffract light at small angular separations, and therefore allow full coronagraphic imaging capability. We show that combining simultaneous astrometric and coronagraphic measurements allows improved detection and characterization of exoplanets by constraining the planet(s) characteristics with both measurements. Our preliminary astrometric accuracy error budget shows that sub-micro arcsecond astrometry can be achieved with a 1.4 m diameter telescope, and that astrometric accuracy improves rapidly with telescope diameter.

Keywords: Astrometry, Exoplanets, Coronagraphy

1. INTRODUCTION

Among the existing techniques to identify exoplanets, astrometry and direct imaging are particularly well suited for identification and characterization of nearby habitable planets. Either technique can provide a full census of habitable planets around nearby (approximately $d < 10pc$) F,G,K main sequence stars, provided that it achieves the requires sensitivity (sub-μas single measurement accuracy for astrometry, 10^{-9} raw contrast at $\approx 50mas$ for coronagraphy). Extensive characterization of the exoplanet does require both techniques, which provide complementary information:

- Direct imaging with a high contrast instrument is required to acquire spectra allowing characterization of the planet's atmosphere.[1] Direct imaging also reveals the exoplanet's environment (other planets in the system, structure of the exozodiacal cloud), and allows measurement of the planet's rotation period and weather variability through time photometry.
- Astrometry[2] is the most promising technique to measure the mass of nearby exoplanets down to a fraction of an Earth mass, and this measurement is required to gain a physical understanding of the planet's surface and atmosphere.

Further author information: (Send correspondence to O.Guyon)
O.Guyon: E-mail: guyon@naoj.org

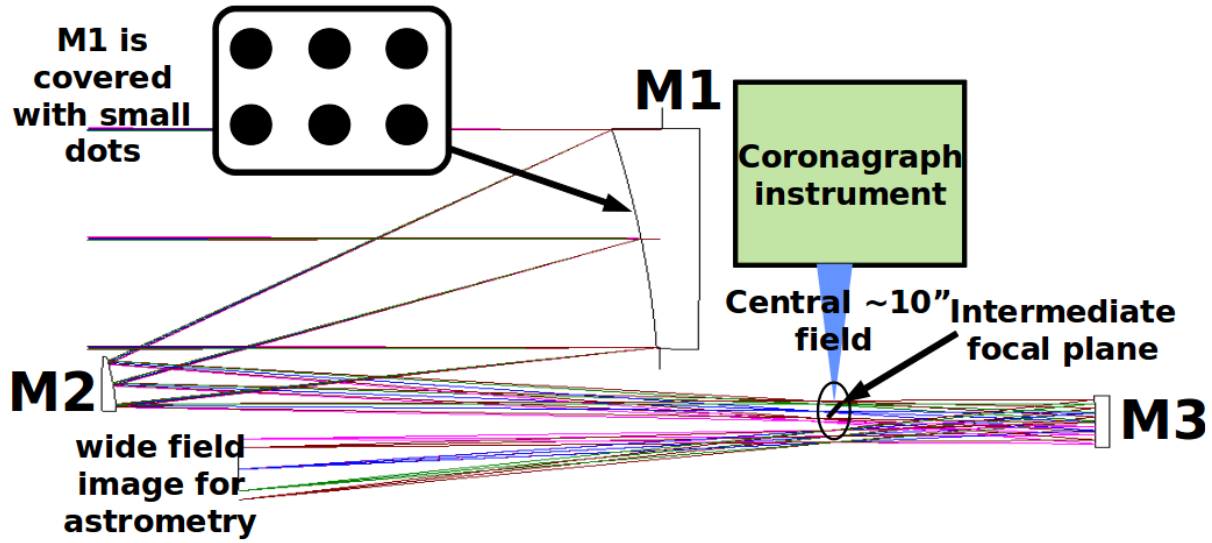

Figure 1. Telescope architecture for simultaneous coronagraphic imaging and astrometry. The design shown in this figure is for a 1.4-m telescope, and offers less than 10-nm wavefront error in a 0.4 deg diameter field. The telescope primary mirror is covered with small dots to create the diffraction spikes used for the astrometric measurement.

Proper interpretation of the planet's photometry and spectra may be challenging without knowledge of the planet's mass, especially for low mass potentially habitable planets for which the data acquired with direct imaging may not offer the signal-to-noise (SNR) ratio required for unambiguous interpretation of spectra. The planet's ability to retain an atmosphere and the atmosphere composition are strong functions of its mass. For low-mass planets, light observed by direct imaging may originate from the planet's surface, while planets with mass larger than a few Earth mass will retain a Hydrogen and Helium rich atmosphere. Both techniques are therefore extremely valuable for characterization of exoplanets.[3]

We discuss in this paper an approach that allows both measurements to be performed simultaneously with the same telescope. The technique relies on diffraction by a grid of dots on the telescope primary mirror.[4] We describe in section 2 how the measurement is performed. In section 3, its performance is discussed, using simulated observations of a planetary system to illustrate the scientific benefit of performing both astrometric and coronagraphic measurements simultaneously.

2. ASTROMETRY WITH A DIFFRACTIVE PUPIL

2.1 Optical principle

As shown in Figure 1, the proposed technique uses a wide field diffraction-limited imaging telescope to simultaneous high contrast coronographic imaging of exoplanet(s) around a target star and high precision measurement of the position of the target star on the sky (absolute astrometry). The central portion of the field is used for coronagraphy and reflected into a coronagraph instrument by a small pickoff mirror. The rest of the field is imaged by a wide field diffraction-limited camera which uses faint background stars as an astrometric reference. By putting dots on the primary mirror, diffraction spikes are created in the wide field astrometric image to provide a suitable reference (linked to the central star) against which the position of the background stars is accurately measured.

The relationship between the pattern of dots on the primary mirror and the diffraction spikes in the focal plane is illustrated in Figure 2, which shows a realistic dot geometry on the primary mirror (left) and the corresponding wide field PSF. The spikes are highly elongated in this polychromatic light simulation. They are also of comparable surface brightness than faint background stars used for the astrometric measurement, and

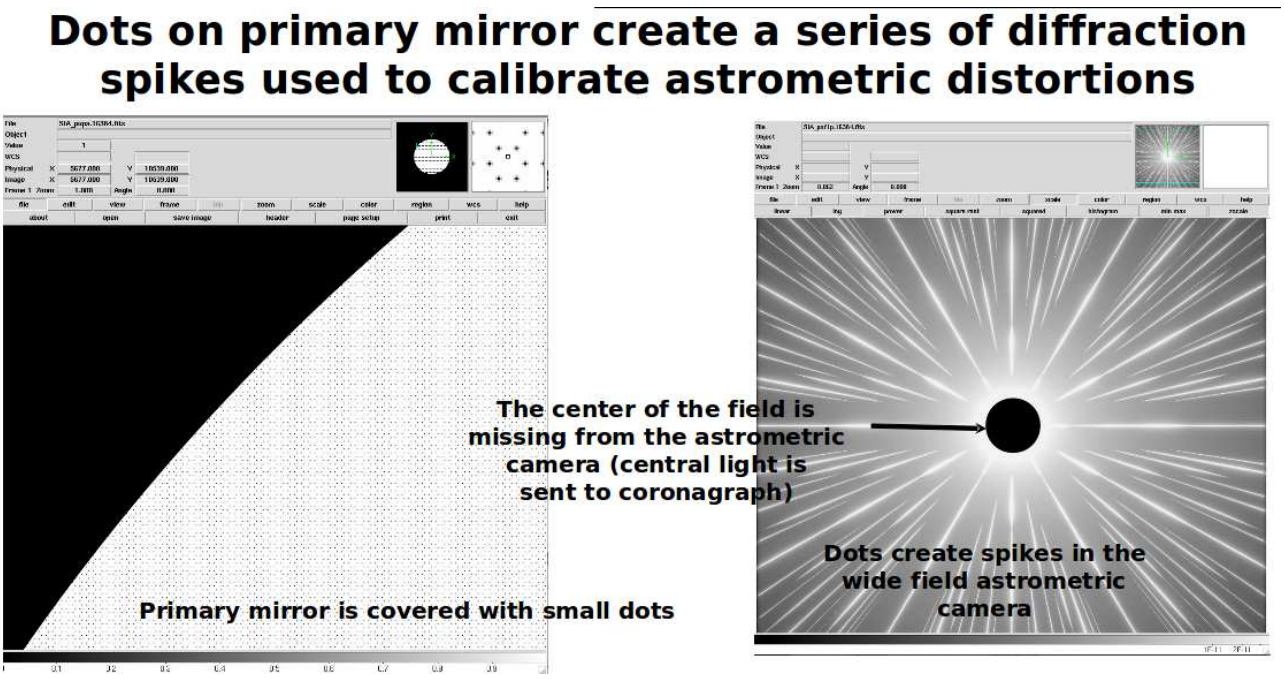

Figure 2. Dots on the telescope primary mirror (left) and corresponding on-axis PSF in the wide field astrometric camera.

since the central bright star is blocked by the coronagraph pickoff mirror, there is no contrast challenge in imaging simultaneously the spikes and the background stars. The astrometric measurement is performed by comparing the motion, between different observing epochs, of the diffraction spikes against the background field stars. We note that a similar magnitude compensation scheme using a grating in front of the telescope has previously been used over small angles for ground-based astrometry of binary stars,[5] and more recently with a grating in a relay pupil for coronagraphic imaging and astrometry of faint companions with adaptive optics.[6,7]

We note that this concept is compatible with both coronagraphy and deep wide field imaging:

- Since the dot pattern on the primary mirror is a regular grid, it does not contain low spatial frequencies, and the diffraction spikes therefore do extend to the central coronagraphic field of view
- The area between the spikes, which is almost all of the focal plane area, is extremely dark, even when the telescope is observing a bright star. In a deep image, the surface brightness between the spikes is dominated by the zodiacal background. The total light in the spikes is also small (at the percent to few percent level), so the dots have little effect on the telescope's sensitivity.

2.2 Calibration of astrometric distortion

While in principle wide field imaging systems provide sufficient field stars for a highly accurate astrometric reference, astrometric distortions due to optics and detector geometry are well above the μas level accuracy we seek. The key to performing high precision astrometric measurement with our technique is that the diffraction spikes will experience the same distortions as the field stars, so a differential astrometric measurement between the diffraction spikes and the field stars is immune from these distortions, regardless of their origin. For example, pointing error moves the spikes and field stars together. Deformations of the detector array and deformations of optical elements will also affect both image features identically.

Figure 3 illustrates how the spikes allow compensation of distortions. We assume here that the same field, centered on the target star, is imaged at two epochs. In a system free of distortions, comparison between images at the two epochs reveals the target star's astrometric motion easily, as the field stars are uniformly displaced

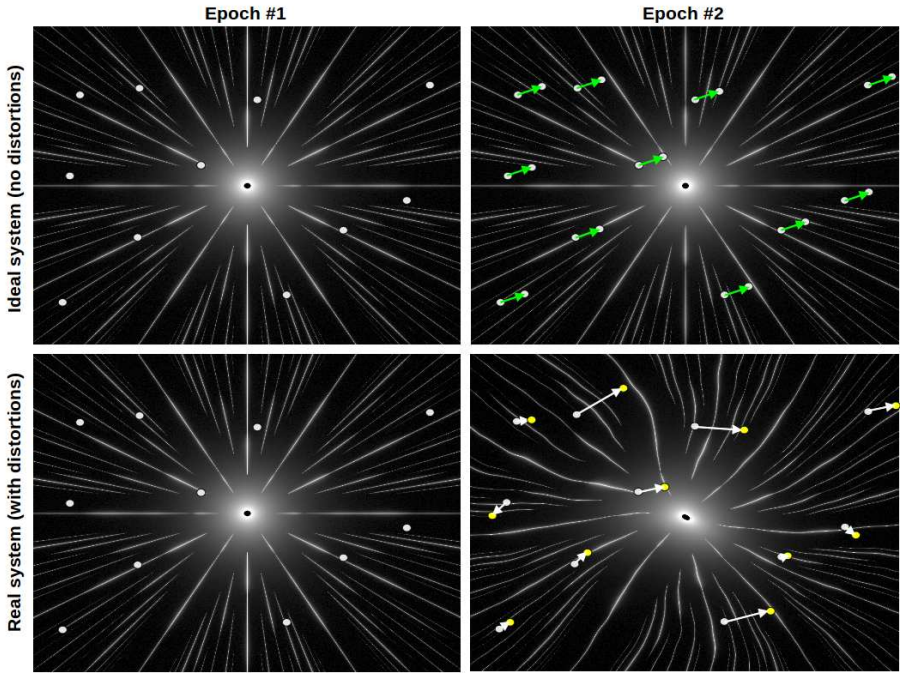

Figure 3. Astrometric measurement without (top) and with (bottom) a differential astrometric distortion between observation epochs.

compared to the spikes. The vectors shows on the top right image show the measured astrometric motion. With astrometric distortions (bottom), the measured displacement of the field stars on the detector is the sum of the true astrometric signal and a (usually much larger) distortion term due to instrumental variations. Since the spikes experience the same distortion, comparison of the spike images between the two epochs reveals the distortion term, which can then be removed from the measurement. Our proposed concept therefore does not require the picometer level stability (or metrology calibration) on the optics over years which would otherwise be essential for wide field astrometric imaging[8,9]

2.3 Other sources of astrometric noise, and mitigation approach

While the diffraction spikes allow measurement and compensation of large scale astrometric distortions, they do not measure small scale (= distortions that vary on a scale smaller than the separation between spikes) astrometric errors. These errors include pixel defects (flat field errors for example), detector geometry errors (such as an unknown discontinuity in pixel size) and small scale optical distortions. The large number of background stars (typically 1000) used for the astrometric reference allows some averaging of these errors (by a factor 30), but these errors are still too large for μas level astrometry even after this averaging.

To further reduce these terms, and achieve sub-μas level astrometry, the telescope can slowly be rolled to move each of the field stars on many pixels. This averaging is extremely efficient on a wide field detector array, where stars can travel over several thousands pixels even with a moderate roll angle. The roll geometry is shown in Figure 4 for two field stars observed at two epochs. The combined averaging due to the large number of stars and large number of independent roll angles for the telescope reduces these error to below μas level for a medium-size telescope.

3. PERFORMANCE

3.1 Astrometric error budget for a 1.4-m telescope

A numerical simulation was developed to quantify the astrometric accuracy of the system. We adopted a 1.4-m diameter telescope with a 0.29 sq.deg field of view astrometric camera for this simulation, and assumed that each

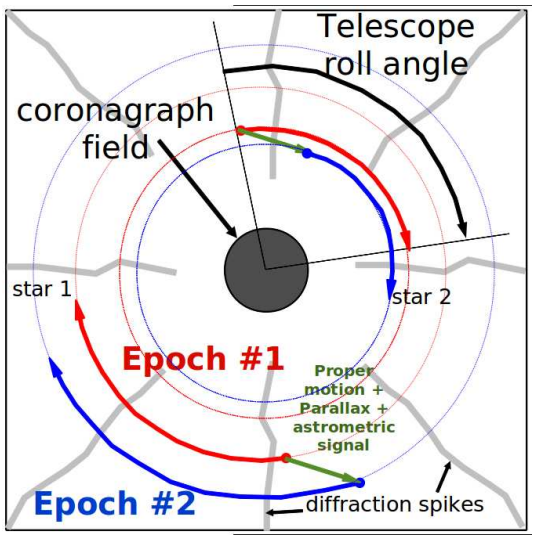

Figure 4. Position of two background stars on the camera focal plane during telescope roll. Observations at two epochs (colored red and blue) are shown for the two stars.

observation was 2-day long. The target is assumed to be a sun-like star at 6pc.

Table 1. Error budget for 1.4-m diameter telescope, 0.29 sq deg field, galactic pole pointing

Photon noise	
Field stars centroid error	0.128 μas
Photon noise on spikes	0.048 μas
Static calibration errors	
Detector flat field	0.033 μas
Optical distortion	0.083 μas
Detector distortion	0.015 μas
Dynamic calibration errors	
Detector flat field	0.029 μas
Optical distortion	0.063 μas
Detector geometry	0.076 μas
TOTAL	0.200 μas

The numerical simulation results, summarized in the error budget in table 1, show that a 0.2 μas astrometric accuracy (1-σ error per measurement per axis for a 2-day observation) is achieved with a 0.29 deg^2 (= 0.6 deg diameter) field of view. The four dominant sources of error are photon noise on the field stars (0.128 μas), static optical distortions (0.083 μas), changes in detector geometry (0.076 μas) and changes in optical distortions (0.063 μas). Together, these four terms contribute to more than 90% of the total astrometric error. Photon noise on the diffraction spikes (0.048 μas), detector flat field errors (0.033 μas), static detector distortion (0.015 μas), and changes in the detector flat field (0.029 μas) are all much smaller.

The fact that the overall contribution of photon noise on field stars (0.128 μas) is comparable to the sum of all other error terms (0.154 μas) is due to the weighting of signals from individual stars in the algorithm. With large calibration errors, the weighting favors a large number of faint stars rather than a small number of bright

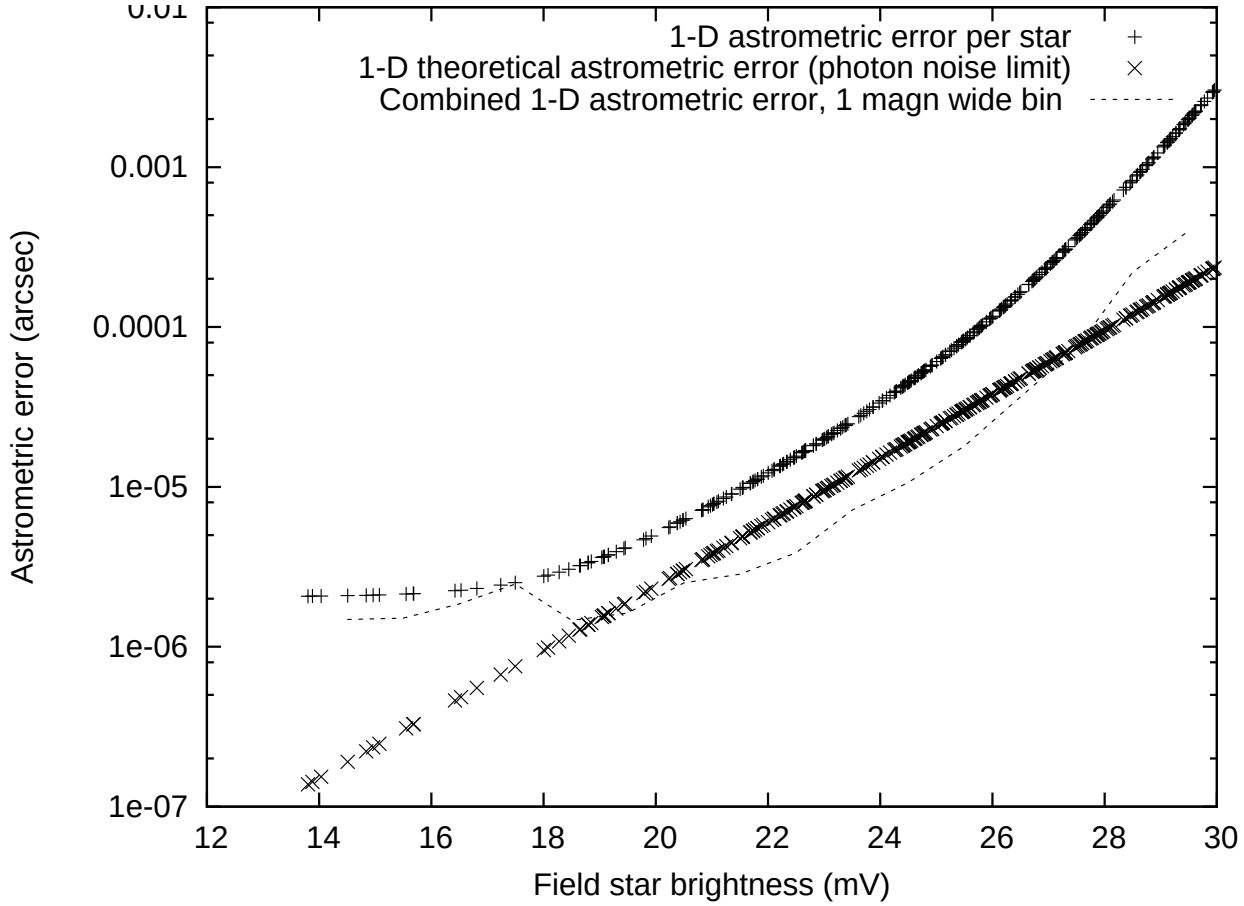

Figure 5. Astrometric 1D error per star on the narrow 0.03 deg^2 (= 0.2 deg diameter) FOV numerically simulated. Each point corresponds to a star in the field. Stars brighter than $m_V = 14$ have been excluded, as they are assumed to be saturated on the detector. The straight line of points shows the expected astrometric error from photon noise alone in monochromatic light ($\lambda = 0.5\mu m$) with infinite pixel sampling and no background. The curved line of points shows the achieved measurement precision, and differs significantly from the photon noise limit both at the bright and faint ends. The dashed curve shows the final 1-D astrometric accuracy obtained if only stars in a 1 magnitude wide brightness bin are used.

stars, which would yield a small photon noise error but a large calibration error due to poor $\sqrt{N}$ averaging. The weighting therefore automatically balances the two error terms, always yielding a field star photon noise contribution approximately equal to the calibration error in the error budget. For a smaller 0.03 deg^2 (= 0.2 deg diameter) field simulated in detail, figure 5 shows the 1-D astrometric error per field star. The final astrometric measurement is obtained by combining 1-D measurements obtained on the field stars with weighting factors chosen to minimize the final error (SNR^2 weighting). Figure 5 shows that the astrometric error is smallest for bright stars, but never goes below ≈ 2 μas due to calibration residuals. For stars fainter than $m_V \approx 18$, photon noise related errors dominate, and the error therefore grows rapidly with stellar magnitude. The figure also shows that, if only stars within a 1 magnitude wide bins were considered, the best astrometric measurement is obtained by selecting stars around $m_V \approx 19$, as this brightness offers the best compromise between number of stars and measurement error per star. Between $m_V \approx 14$ and $m_V \approx 22$, each magnitude bin contributes almost equally to the final astrometric precision, as the decrease in precision per star as stellar magnitude increases is compensated by the increase in numbers of stars.

Figure 5 also shows the theoretical monochromatic astrometric measurement error per star, with the corresponding points aligned on a straight line in the log-log scale. This level of error is achieved if detector spatial sampling is infinite, in monochromatic light in the absence of calibration errors or background. At the bright end of the figure, the achieved error is much larger than this limit due to calibration errors. At the faint end, photon noise of the zodiacal background light dominates the error, as shown by the strong deviation of the curve from the ideal straight line. Even at the intermediate brightness where both zodiacal light photon noise and calibration errors are small compared to the theoretical limit, the achieved measurement error is about twice as large as the $1/(\pi\sqrt{N_{ph}})\lambda/D$ photon noise ideal limit, due to limited pixel sampling and polychromaticity of the PSF.

Figure 5 illustrates the robustness of the concept performance against moderate increases of the sources of calibration noise. If the calibration floor were to be multiplied by two (4 μas instead of 2 μas), the final astrometric measurement error would only increase by a 23 % to 0.246 μas, as a larger number of fainter stars would be selected to mitigate the increased calibration error. The final performance is therefore not highly sensitive to changes in the assumptions made in this paper about optical quality, detector properties and instrument stability. This suggests that obtaining substantially better accuracy than computed in this section would require improvements in the quality and stability of the system which are significantly beyond the realistic assumptions made in this paper. Better astrometric accuracy is therefore likely to require a combination of larger telescope or field of view or modifications of the concept aimed at calibrating some of the dominant sources of calibration error.

3.2 Astrometric precision as a function of telescope size and field of view

Table 2. Expected single measurement astrometric accuracy as a function of telescope diameter and field of view (Galactic pole pointing, 2 day integration)

Diam	**0.03** deg^2	**0.1** deg^2	**0.3** deg^2	**1** deg^2
1.0 m	0.99 μas	0.54 μas	0.31 μas	0.17 μas
1.4 m	0.62 μas	0.34 μas	0.20 μas	0.11 μas
2.0 m	0.38 μas	0.21 μas	0.12 μas	0.066 μas
2.8 m	0.24 μas	0.13 μas	0.076 μas	0.041 μas
4.0 m	0.15 μas	0.081 μas	0.047 μas	0.026 μas
5.7 m	0.092 μas	0.050 μas	0.029 μas	0.016 μas
8.0 m	0.059 μas	0.032 μas	0.019 μas	0.010 μas

The astrometric measurement error is estimated for different values of telescope diameter and field of view in table 2. The numbers shown in the table were derived by separating, for each star in the field, the error into a

photon noise term and a calibration term. The photon noise term includes photon noise from the field star and zodiacal light, and the calibration term is a fixed error per star. The quadratic sum of the two terms matches for the nominal design (D=1.4m, FOV = 0.3 deg^2 = 0.6 deg diameter) the curve obtained in figure 5, and therefore takes into account all sources of error described in this paper. To evaluate how measurement error varies with telescope diameter, we scale for each background star the photon noise error with telescope diameter (this scaling is done separately for photon noise due to zodiacal light and field star photon noise), and we assume that the calibration residual error per star scales as the inverse of telescope diameter. This last assumption is somewhat arbitrary, but can be justified by the fact that the pixel size scales as λ/D, and that the width of the diffraction spikes used for calibration also scales as λ/D. We however note that proper extrapolation of calibration residuals for different telescope diameters requires optomechanical designs for different telescope sizes, and is beyond the scope of this paper. We also note that the results shown in table 2 are not strongly dependent on the calibration error per star, but are in large part driven by the ability to use a large number of fainter stars with the larger telescope sizes, and that this latter effect is well understood and quantified by simple scaling laws.

While the measurement is limited by systematics (scaling as λ/D) for bright field stars, it is limited by photon noise (scaling as λ/D^2) for fainter stars. For a fixed field of view, the overall measurement error dependence on telescope diameter is therefore intermediate between these two scaling laws: with larger telescope diameters, a larger number of fainter stars is used toward the final measurement to overcome the systematics and take advantage of the lower photon noise.

3.3 Observation of planetary systems with simultaneous coronagraphy and astrometry

We have simulated observation of a planetary system consisting of 3 planets around a Sun-like star at 6pc. The 3 planet masses and separations are:

- Planet 1: 1 M_{Earth}, 1.2 AU
- Planet 2: 4 M_{Earth}, 1.8 AU
- Planet 3: 16 M_{Earth}, 2.4 AU

For simplicity, the orbits are assumed to be circular and coplanar. We assume that the planetary system is observed with a 1.4-m diameter telescope equipped with a coronagraph offering a 2 λ/D inner working angle (planets are only visible if outside this separation) at 0.5 μm, and an astrometric measurement capability with 0.2 μas per measurement (1 axis standard deviation), as detailed in our previous example.

To illustrate the complementarity of astrometric and coronagraphic measurements, and the value of performing both measurements simultaneously, we have simulated 3 different mission scenarios:

- Coronagraphic measurement only: the planet is imaged only when outside the coronagraph's IWA (the inner planet is sometimes invisible due to inclination of the orbital plane), and its position relative to the star is then measured. One coronagraphic observation is done every 2 month
- Astrometry only: One observation is performed every month, with an 0.2 μas precision per axis.
- Astrometry + coronagraphy: Every 2 month, an astrometric measurement at the 0.2 μas precision per axis and a coronagraphic observation are performed.

Results are shown in figure 6, and demonstrate that our proposed combined coronagraphy + astrometry approach is very powerful at identifying planets in a multiplanet system, and constraining their masses. For a one year mission, the Earth-mass planet in the system is already identified as a potentially habitable planet, and would then be observed at higher cadence and SNR in a mission dedicated to characterizing habitable planets. With the astrometry only mission, it would take approximately 4 years to constrain the planet mass to the same level.

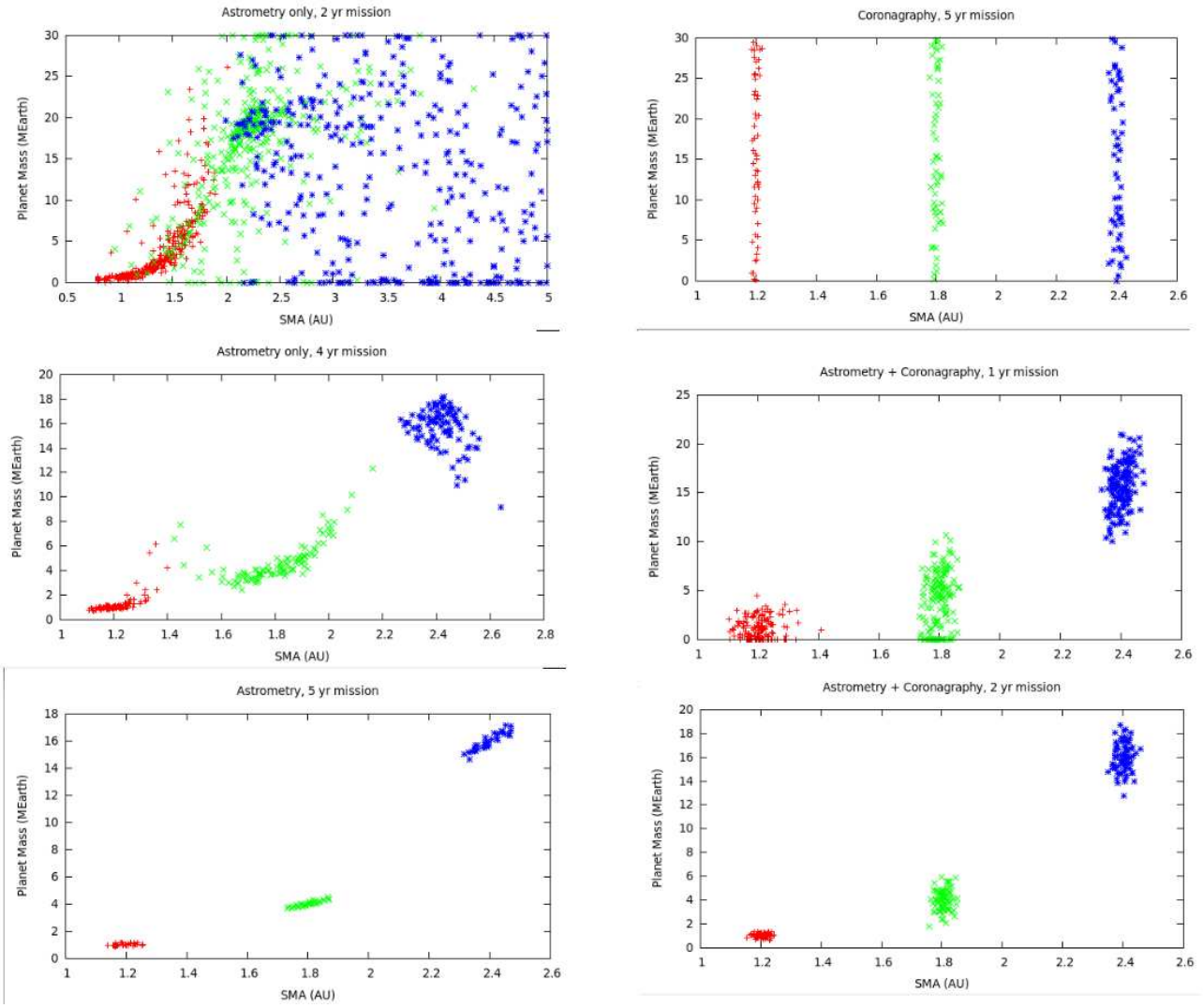

Figure 6. Result of different mission scenario, observing a 3 planet system around a Sun like star at 6pc. For each case, many realization of the observations are performed, and the best 3-planet solution is shown in the semi-major axis (x axis) - mass (y axis) plane. Left column: astrometric mission, with a total mission duration ranging from 2 yr (top) to 5 yr (bottom). Top right: coronagraphic mission. Middle right and bottom right: combined astrometry + coronagraphy mission. This figure demonstrates that performing simultaneous coronagraphy and astrometry is very efficient at measuring planets parameters, even in a short duration mission.

4. CONCLUSION

The diffractive pupil telescope concept described in this paper is an attractive solution to perform, in a single mission, simultaneous coronagraphic imaging and astrometric mass determination of exoplanets around nearby stars. We have shown that the diffractive primary mirror can be designed to allow unperturbed coronagraphic imaging of the central field and full sensitivity wide field imaging for other astrophysical investigations. The concept is especially attractive if a coronagraphic instrument is installed on a wide field imaging telescope, as the change required to perform astrometric measurement (addition of dots on the primary mirror) is of moderate cost and will not strongly impact other science goals. Simultaneous high precision astrometry and coronagraphic imaging is a powerful combination for the identification and characterization of exoplanets, with a total scientific return exceeding the sum of what can be derived separately from the two individual measurements. Our preliminary analysis indicates that with a 0.3 deg^2 field of view camera on a 1.4-m telescope, the astrometric accuracy can reach 0.2 μas per 2-day measurement, sufficient to measure exoplanet masses to 0.1 M_{Earth} precision in the habitable zone of nearby stars. Performance is expected to improve rapidly with telescope size, and could be further enhanced with additional metrology hardware, environment control and software removal of instrumental errors identified by careful analysis of data acquired through the mission duration.

We are currently developing a laboratory testbed of the concept. Data reduction algorithms will be developed and tested, and laboratory data will increase our ability to link telescope stability and optical quality to astrometric performance. Accurate estimation of the astrometric accuracy will also require detailed modeling of the spacecraft and telescope stability over long timescales.

ACKNOWLEDGMENTS

This work was funded by NASA and the University of Arizona.

REFERENCES

[1] Levine, M., Lisman, D., Shaklan, S., Kasting, J., Traub, W., Alexander, J., Angel, R., Blaurock, C., Brown, M., Brown, R., Burrows, C., Clampin, M., Cohen, E., Content, D., Dewell, L., Dumont, P., Egerman, R., Ferguson, H., Ford, V., Greene, J., Guyon, O., Hammel, H., Heap, S., Ho, T., Horner, S., Hunyadi, S., Irish, S., Jackson, C., Kasdin, J., Kissil, A., Krim, M., Kuchner, M., Kwack, E., Lillie, C., Lin, D., Liu, A., Marchen, L., Marley, M., Meadows, V., Mosier, G., Mouroulis, P., Noecker, M., Ohl, R., Oppenheimer, B., Pitman, J., Ridgway, S., Sabatke, E., Seager, S., Shao, M., Smith, A., Soummer, R., Stapelfeldt, K., Tenerell, D., Trauger, J., and Vanderbei, R., "Terrestrial Planet Finder Coronagraph (TPF-C) Flight Baseline Concept," *ArXiv e-prints* (2009).

[2] Shao, M., Marcy, G., Catanzarite, J. H., Edberg, S. J., Léger, A., Malbet, F., Queloz, D., Muterspaugh, M. W., Beichman, C., Fischer, D., Ford, E., Olling, R., Kulkarni, S., Unwin, S. C., and Traub, W., "Astrometric Detection of Earthlike Planets," in [*astro2010: The Astronomy and Astrophysics Decadal Survey*], *Astronomy* **2010**, 271–+ (2009).

[3] Shao, M., Catanzarite, J., and Pan, X., "The Synergy of Direct Imaging and Astrometry for Orbit Determination of Exo-Earths," *ApJ* **720**, 357–367 (2010).

[4] Guyon, O., Shao, M., Shaklan, S., Levine, M., Ammons, M., Bendek, E., Woodruff, R., Nemati, B., and Pitman, J., "Single aperture imaging astrometry with a diffracting pupil: application to exoplanet mass measurement with a small coronagraphic space telescope," *Society of Photo-Optical Instrumentation Engineers (SPIE) Conference Series* **7731** (2010).

[5] Strand, K. A., "Photographic observations of double stars made with the 24-inch Sproul refractor," *AJ* **52**, 1–+ (1946).

[6] Sivaramakrishnan, A. and Oppenheimer, B. R., "Astrometry and Photometry with Coronagraphs," *ApJ* **647**, 620–629 (2006).

[7] Zimmerman, N., Oppenheimer, B. R., Hinkley, S., Brenner, D., Parry, I. R., Sivaramakrishnan, A., Hillenbrand, L., Beichman, C., Crepp, J. R., Vasisht, G., Roberts, L. C., Burruss, R., King, D. L., Soummer, R., Dekany, R., Shao, M., Bouchez, A., Roberts, J. E., and Hunt, S., "Parallactic Motion for Companion Discovery: An M-Dwarf Orbiting Alcor," *ApJ* **709**, 733–740 (2010).

[8] Unwin, S. C., "Precision Astrometry with the Space Interferometry Mission - PlanetQuest," in [*Astrometry in the Age of the Next Generation of Large Telescopes*], P. K. Seidelmann & A. K. B. Monet, ed., *Astronomical Society of the Pacific Conference Series* **338**, 37–+ (2005).

[9] Meijer, E. A., Nijenhuis, J. N., Vink, R. J. P., Kamphues, F., Gielesen, W., and Coatantiec, C., "Picometer metrology for the GAIA Mission," *Society of Photo-Optical Instrumentation Engineers (SPIE) Conference* **7439** (2009).